 MCB, vol.9, no.2, pp.95-125, 2012

3D Numerical Study of Tumor Microenvironmental Flow in Response to Vascular-Disrupting Treatments

Jie Wu[*,†], **Yan Cai**[‡], **Shixiong Xu**[§], **Quan Long**[¶], **Zurong Ding**[*]
Cheng Dong[*,‖]

Abstract: The effects of vascular-disrupting treatments on normalization of tumor microvasculature and its microenvironmental flow were investigated, by mathematical modeling and numerical simulation of tumor vascular-disrupting and tumor haemodynamics. Four disrupting approaches were designed according to the abnormal characteristics of tumor microvasculature compared with the normal one. The results predict that the vascular-disrupting therapies could improve tumor microenvironment, eliminate drug barrier and inhibit metastasis of tumor cells to some extent. Disrupting certain types of vessels may get better effects. In this study, the flow condition on the networks with "vascular-disrupting according to flowrate" is the best comparing with the other three groups, and disrupting vessels of lower maturity could effectively enhance fluid transport across vasculature into interstitial space.

Keywords: Solid tumor, vascular-disrupting, microenvironment normalization, haemodynamics, 3D numerical simulation.

1 Introduction

Antitumor therapies rely on the transport of therapeutic medicines or diagnostic agents to tumor cells via the blood stream and tumor interstitium. Unlike normal blood vessels, tumor vasculature has abnormal organization, structure, and

[*] School of Naval Architecture, Ocean and Civil Engineering, MOE Key Laboratory of Hydrodynamics, Shanghai Jiao Tong University, Shanghai, China
[†] Corresponding author. Email: jiewu82@sjtu.edu.cn; Phone: +86-021-34204313, +86-13564458476
[‡] School of Biological Science and Medical Engineering, Southeast University, China
[§] Department of Mechanics and Engineering Science, Fudan University, Shanghai, China
[¶] Brunel Institute for Bioengineering, Brunel University, Uxbridge, Middlesex, UK
[‖] Department of Bioengineering & Department of Engineering Science and Mechanics, The Pennsylvania State University, The Pennsylvania State, USA

function. Vascular hyperpermeability and the lack of functional lymphatic vessels inside tumors cause elevation of interstitial fluid pressure (IFP) in solid tumors [1]. The elevated tumor IFP increases fluid flow from the tumor margin into the peri-tumor area and may facilitate peri-tumor lymphatic hyperplasia and metastasis. These characteristics cause abnormal microenvironment in tumors and form a physiological barrier to the delivery of therapeutic agents to tumors [1,2].

In recent years, tumor vascular-targeted therapies have been extensively studied, including "anti-angiogenesis" and "vascular-disrupting" treatments. Anti-angiogenesis treatments directly targeting angiogenic signaling pathways as well as indirectly modulating angiogenesis. Vascular-disrupting treatments target the established tumor vasculature. Some vascular-disrupting agents have been proven to effectively disrupt or prune vessels in tumor vascular system. However, the current understanding of how microenvironmental flow is affected by vascular-targeted therapies is limited since imaging resolution is not adequate to reveal the fine details of tumor microvessel. Particularly, according to a recent literature [1], there are no reported measurements of interstitial fluid velocity in tumors, since the experimental data are difficult to obtain. Therefore, numerical simulation can play an important role on study. Few model of tumor vascular-disrupting has been developed so far. Neither does the study of tumor haemodynamics on vascular-disrupting networks. The aim of this paper was to investigate the effects of vascular-disrupting treatments on tumor microvasculature and resultant microenvironment normalization. Four disrupting approaches were designed according to the abnormal characteristics of tumor microvaculature compared with the normal one. The flow simulations were carried out on these networks and the results were compared with that on the "unnormalized" ones. Fig. 1 describes the major structure of the study. It is based on the mathematical models of (1) tumor angiogenesis; (2) vascular-disrupting; and (3) tumor haemodynamics. In the discussion section, the model validation was made through the comparison of the flow simulation results with the clinical MRI results, also the flow change response to the changes of transport properties of tumor vessels and tissue was analyzed.

2 Models and methods

2.1 Model of tumor vascular-disrupting

Some vascular-disrupting agents have been proven to effectively discrupt or prune vessels in tumor vascular system. Here, four vascular-disrupting approaches are designed, according to the abnormal characteristics of tumor vaculature. The original vascular network is obtained from the 3D model of tumor angiogenesis [3,4]. Fig. 2a and Fig. 2b show the model scheme and the generated network respectively.

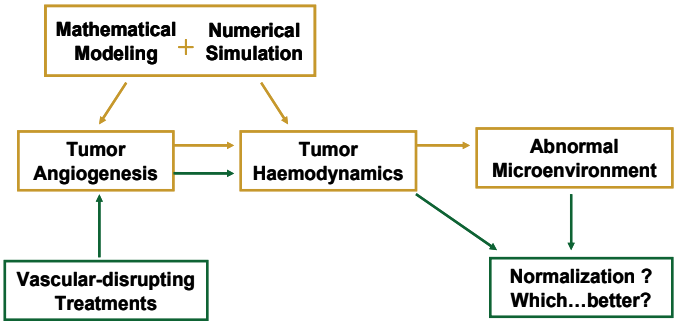

Figure 1: The structure of the study.

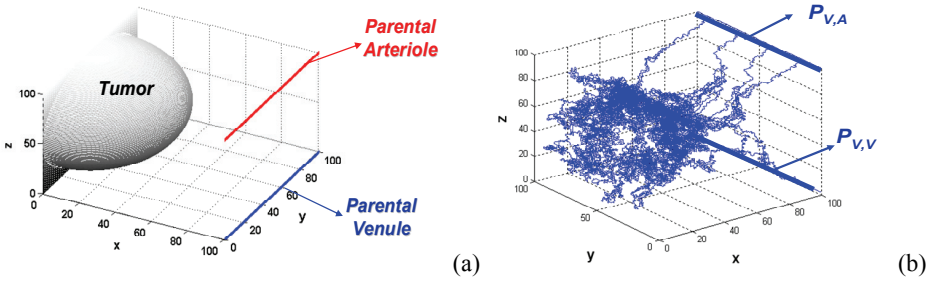

Figure 2: (a) 3D model scheme of tumor angiogenesis; (b) 3D vascular network from the angiogenesis simulation.

The network is induced from an arteriole and a venule of the host as two parental vessels, and the examination of vessel connectivity has been carried out to guarantee the efficiency of blood flow through the network. The detailed description of the model can be found in Appendix A.

2.1.1 Disrupting randomly

In this approach, the vessels are disrupted randomly from the original vascular network, and those vessel segments no longer forming loops for effective blood flow are removed. As shown in Fig. 3, 'Network 2(R)', 'Network 3(R)', 'Network 4(R)' are obtained by disrupting randomly of 'Network 1', 'Network 2(R)' and 'Network 3(R)' respectively. 'Network 1' is the oringinal network, the same one in Fig. 2b.

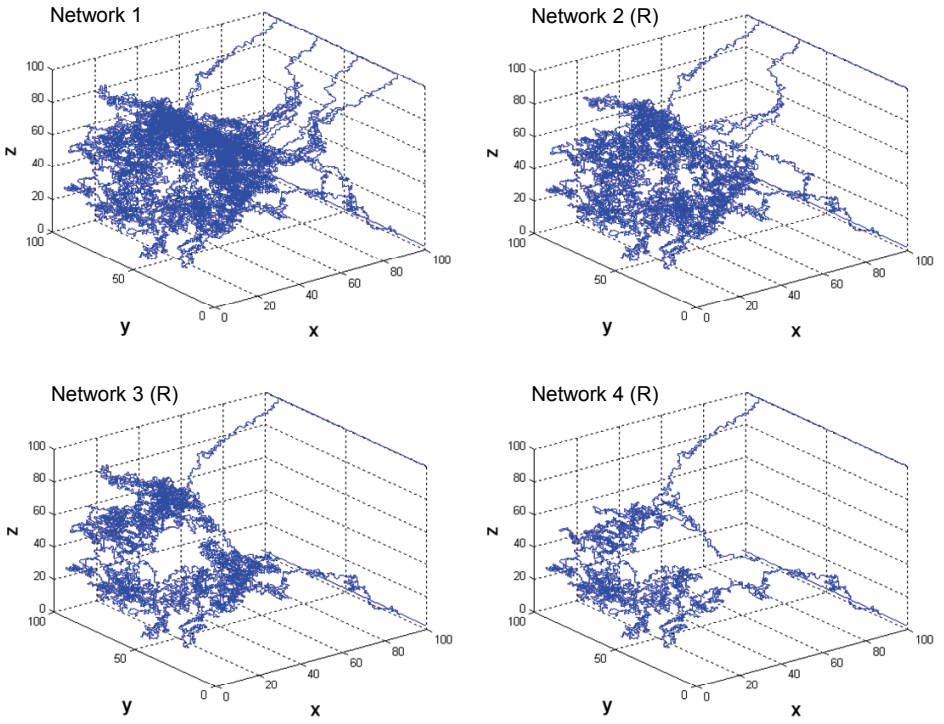

Figure 3: Simulation results of vascular-disrupting randomly.

2.1.2 *Disrupting according to network structure*

It is believed that trifurcations is one typical network structure abnormality of tumor vessels, which will influence blood perfusion in tumors [5,6,7]. Here, one "normalization" procedure considered is to cut the trifurcations and remove the residual vessel segments accordingly. Another abnormality of tumor vasculature structure is vessels being twisted and tangled with each other [2,8,9], also, which will be pruned to be normalized in this study. Fig. 4 presents the processed networks, 'Network 2(S)' is obtained by pruning the vessels having trifurcations branches of 'Network 1'; 'Network 3(S)' is from disrupting those twisted vessels (more than three that twist together) of 'Network 1'; 'Network 4(S)' is the result from the combination of the above two cutting processing.

2.1.3 *Disrupting according to vessel maturity*

Immature vessels in tumor will not only help local spread of cancer cells, but also promote cancer cell infiltration through its own protease partial role. Studies have

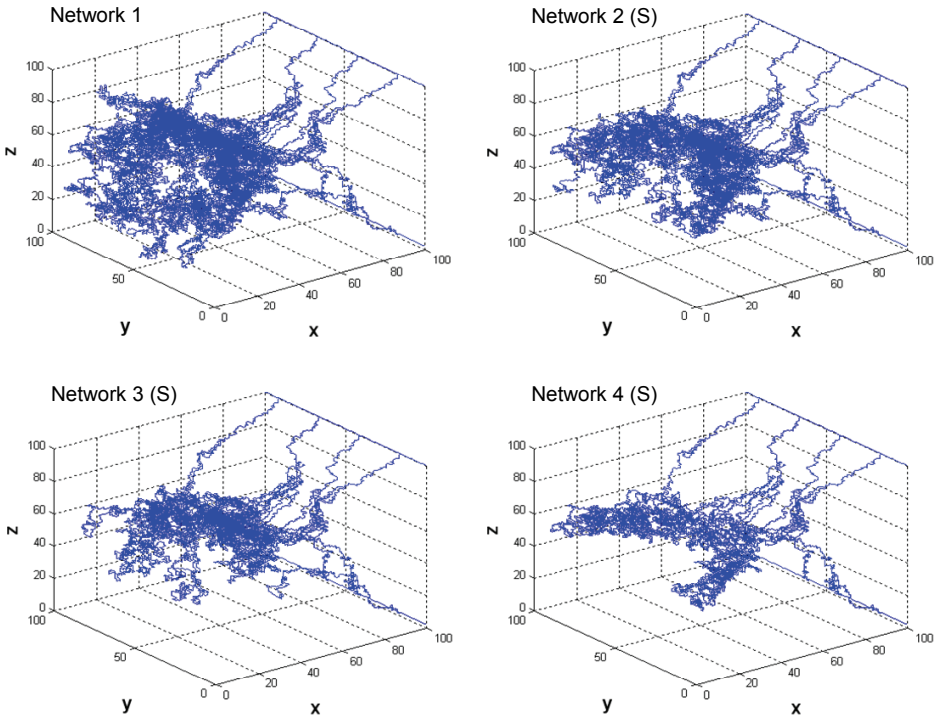

Figure 4: Simulation results of vascular-disrupting according to network structure.

shown that, the treatment will be more effective than expected if the high proportion of immature vessels inside tumor are destroyed [10]. Actually, vascular-disrupting agents have been developed for rupturing the rapidly proliferated and immature vascular endothelial cells, thereby block the low mature vessels inside of tumor [11,12]. In this study, we consider the growing time of vessels as a criterion of its maturity. As shown in Fig. 5, 'Network 2(M)', 'Network 3(M)', 'Network 4(M)' are obtained from cutting off the vessels in 'Network 1' with a growing time less than 5 days, 10 days and 15 days, respectively. The growing time for a 'Network 1' is 24 days.

2.1.4 Disrupting according to blood flowrate

The researches have predicated that anti-tumor drugs can damage some immature blood vessels, and these vessels are often with lower blood flowrate [13]. Accordingly, we design the fourth approach—disrupting according to blood flowrate. Fig. 6 shows the simulation results, 'Network 2(F)', 'Network 3(F)' and 'Network 4(F)'

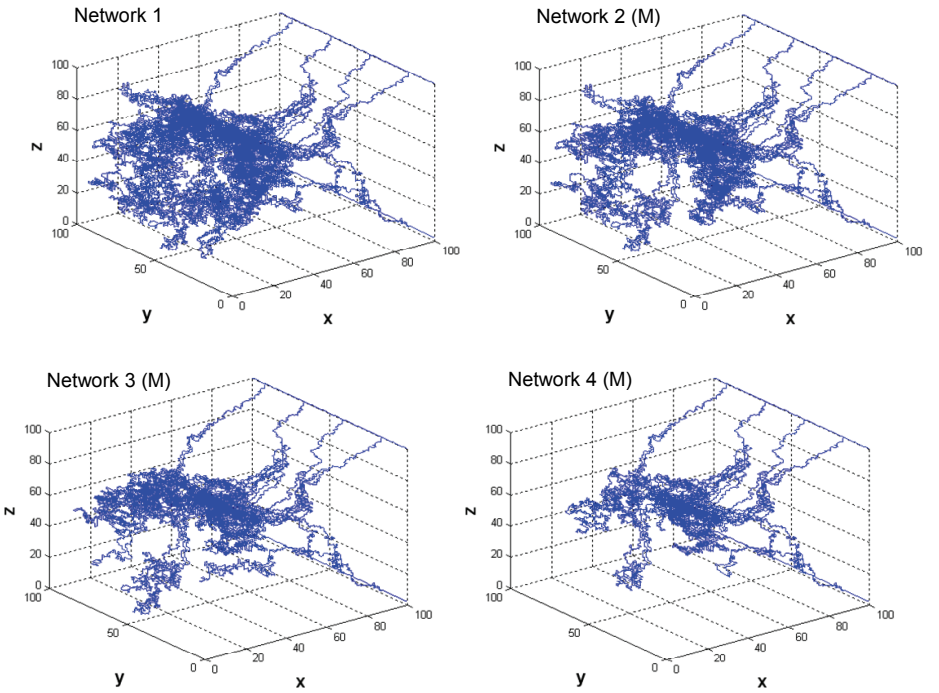

Figure 5: Simulation results of vascular-disrupting according to vessel maturity.

are obtained by pruning the vessels, in which the blood flowrate is less than 20%, 40%, and 60% of the average blood flowrate on 'Network 1', respectively.

2.2 Model of tumor haemodynamics

The flow model incorporates (a) intravascular blood flow; (b) transvascular leakiness; (c) interstitial fluid movement; (d) blood rheology; (e) vessel compliance; (f) lymphatic absorption, as shown in Fig. 7. The detailed description of the flow model can be found in our recent published articles [4,14]. Briefly, for the intravascular blood flow, the basic equation is the flux conservation and incompressible flow at each node. Flow resistance is assumed to follow Poiseuille's law in each vessel; the transvascular flow rate is controlled by starling's law; Darcy's law is used to calculate the interstitial fluid flow. The intravascular and interstitial flow is coupled by the transvascular flow. In addition, blood viscosity is calculated based on the the formula developed by Pries et al. (1994) [15], in which blood viscosity is the function of vessel diameter, local hematocrit, and plasma viscosity. It is assumed the blood vessels at outside of the tumor are rigid, the vessel compliance within the

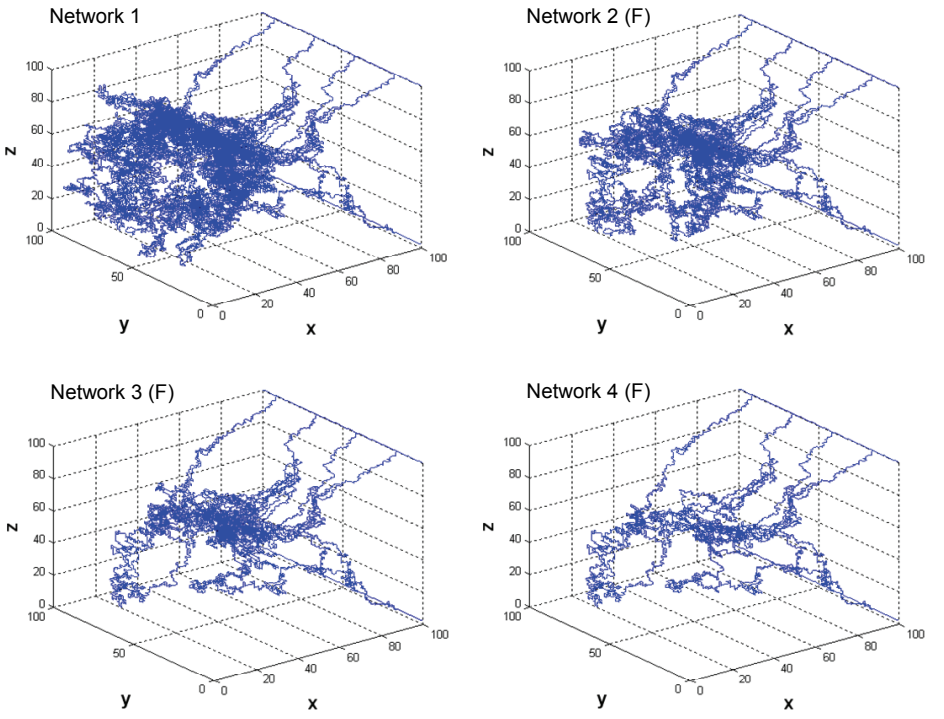

Figure 6: Simulation results of vascular-disrupting according to blood flowrate.

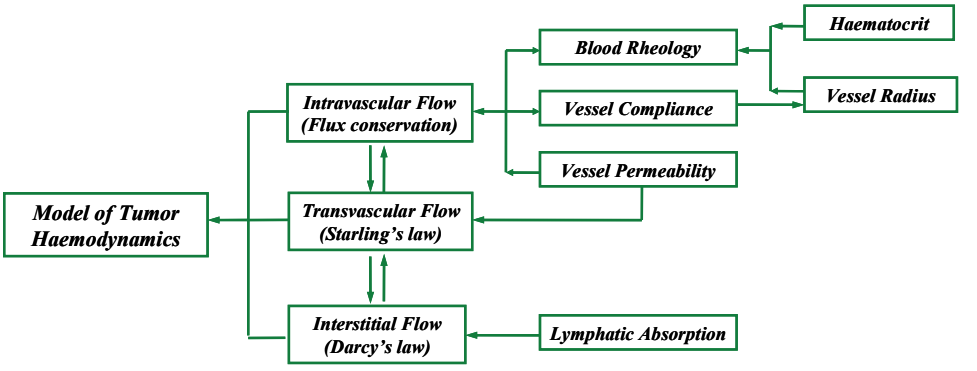

Figure 7: Schematic structure of the flow model.

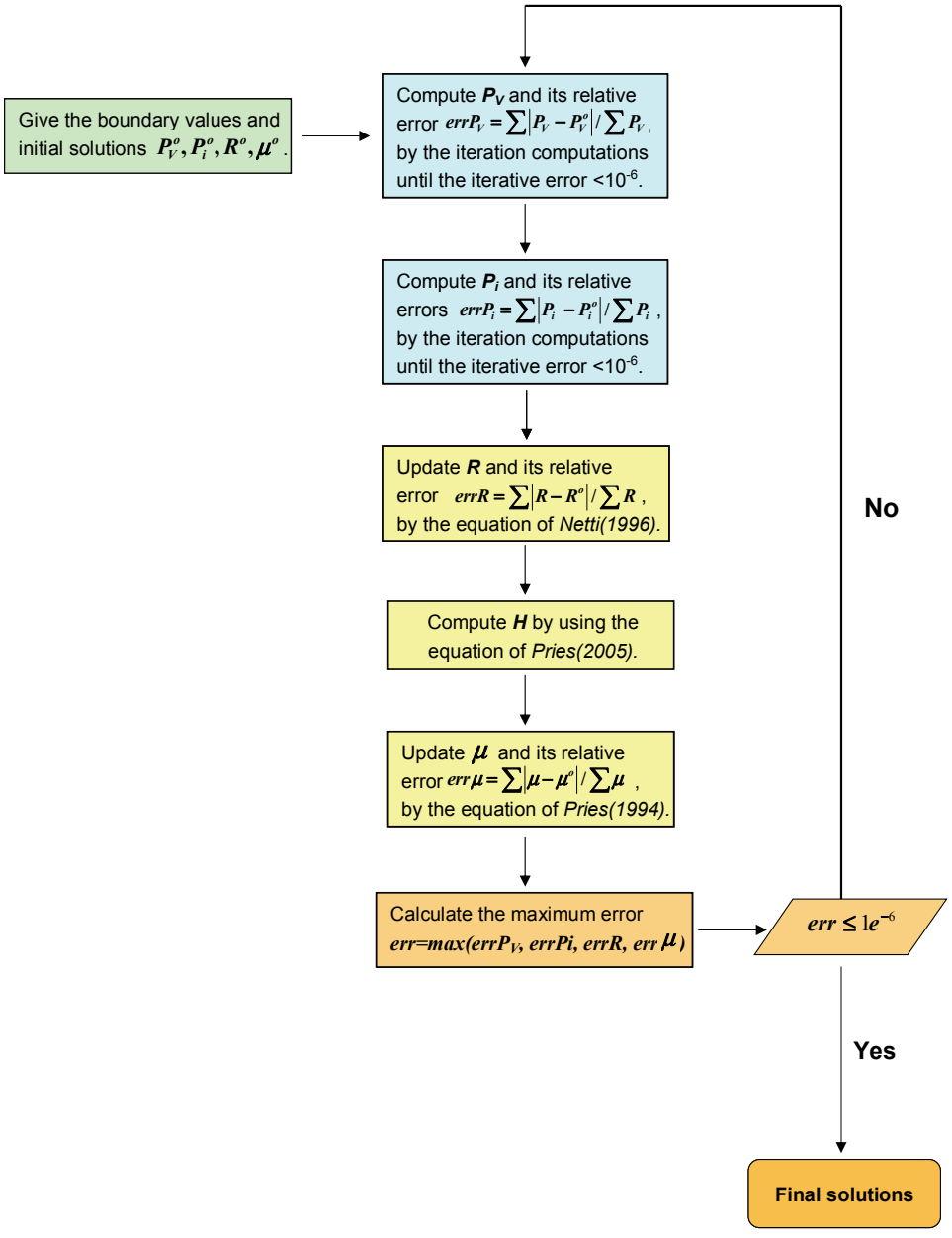

Figure 8: Schematic structure of the iterative numerical procedure.

tumor is calculated based on the equation of Netti et al. (1996) [16]. The distribution of red blood cells (RBCs) at microvascular bifurcations is represented according to the approach proposed by Pries & Secomb (2005)[17]. The above governing equations are listed in Appendix B.

In the flow simulations, the pressure of the arteriole and venule parental vessels are given $P_{V,A}$=25mmHg, $P_{V,V}$=10mmHg, see Fig. 2b. The other parameter values can be found in the papers [4,14]. A specific coupling procedure is developed in the study to couple the intravascular and interstitial flow. It is based on the iteratively numerical simulation techniques, including local iterations at individual parameter level and one global loop to provide coupling and control of the simulation convergence. The schematic structure of the interative numerical procedure is shown in Fig. 8.

3 Simulation results

3.1 Flows on the oringinal vasculature without vascular-disrupting treatment

Fig. 9 shows the flow simulation results on the oringinal network 'Network 1'(the control one), figure (a)∼(e) are the distributions of intravascular pressure P_V, intravascular velocityU_V, transvascular velocity U_t, interstitial pressure P_i and interstitial velocity U_i, respectively. Three curves are presented in each figure, corresponding to the groups of arterioles, venules and capillaries. The vessel classification could be found in [4].

According to Fig. 9a and Fig. 9b, P_V almost remains constant in the tumor interior region, U_V in the intra-tumoral vessels is much lower than those outside the tumor, especially, in the intra-tumoral capillaries, the blood flows extremely slowly. In Fig. 9c, extravasation flow (or outward flow from blood vessels) is defined as positive (U_t^+) while intravasation (or inward flow) as negative (U_t^-). Due to the much higher permeability of tumor vessels, transvascular flow in the normal tissue can be negligible compared with that inside the tumor. A relatively large value of extravasation (U_t^+) is presented at the tumor periphery, also, the elevated P_i inside the tumor causes the intravasation phenomena (U_t^-). The simulation results also show that the transvascular flux is as the same magnitude of the intravascular flux, the ratio of the total amount of intravasation flux to extravasation flux is about 16%. As shown in Fig. 9d, a plateau of P_i is found in the interior of the tumor, which drops rapidly at the periphery. Fig. 9e shows the distribution of U_i (the flow of outward tumor centre direction is positive). It is noteworthy that, U_i is very slow inside the tumor due to the low gradient of P_i, which may provide resistance for drug delivery. On the other hand, at the tumor periphery, U_i becomes much larger due to the very high gradient of P_i, so a large amount of interstitial fluid is

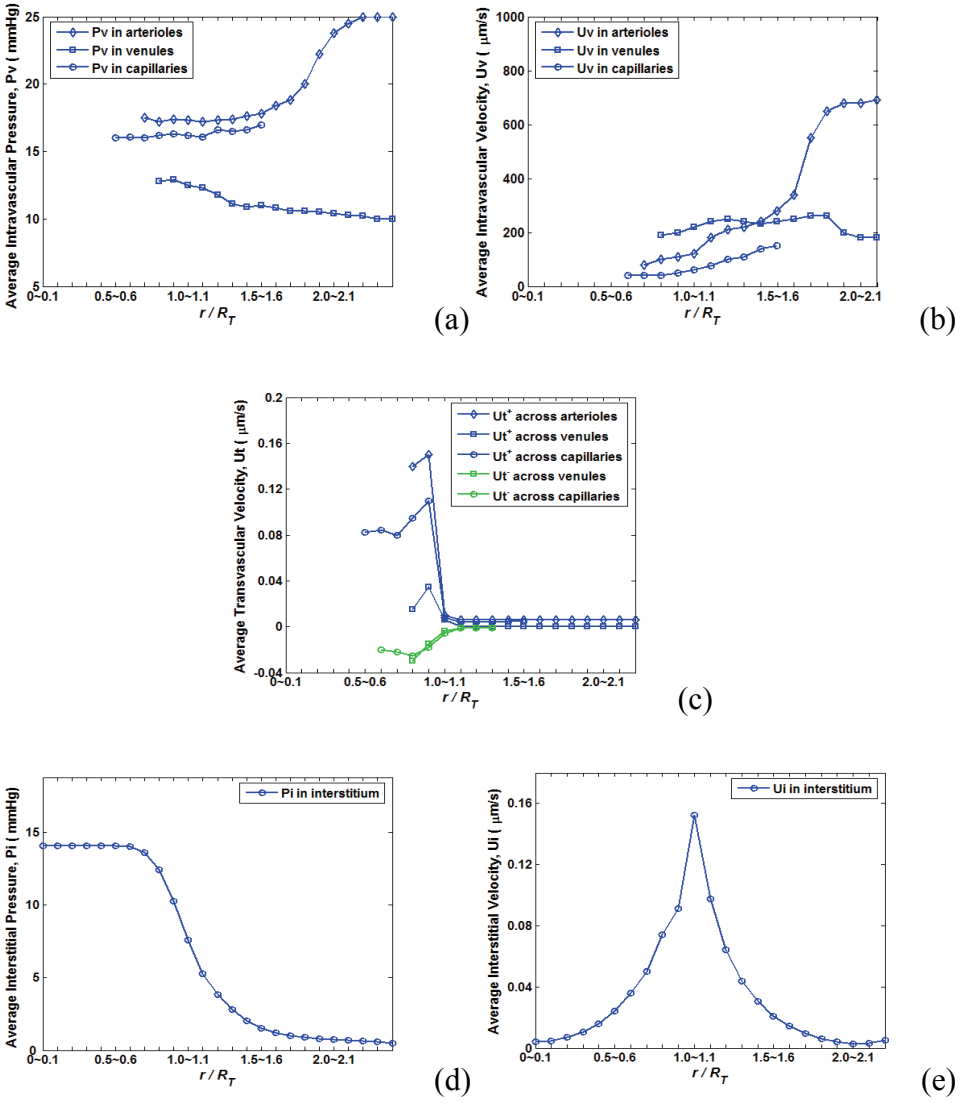

Figure 9: 3D flow simulation results of the control group (on Netowrk 1). The distributions of the (a) intravascular pressure $P_V(mmHg)$; (b) intravascular velocity $U_V(\mu m/s)$; (c) transvascular velocity $U_t(\mu m/s)$; (d) interstitial pressure P_i $(mmHg)$; (e) interstitial flow velocity U_i $(\mu m/s)$. ($x-$ axis represents the normalized distance from the tumor centre to the parent vessels, where R_T is the tumor radius, r/R_T = 0.0, 1.0 correspondents to the tumor centre and boundary respectively.)

discharged out of the tumor and enters into the host tissues which may speed the drug to be drained into peritumor lymphatic vessels into the host tissues.

3.2 Flows n the "vascular-disrupting" microvasculatures

In the below figures, each data is the calculated mean value based on 30 simulated networks of the corresponding disrupting approach, to provide a general trend of the flows. We use the flow values before the treatment as the baseline value (the results in Sec 3.1), and make comparisons with the corresponding results on those disrupting networks.

The comparisons of the flow values on the four groups of disrupting vasculatures are listed in Tab. 1, $Q_V/Q_{V(Net.1)}$: the relative value of total blood perfusion through the vasculature, $Q_t^+/Q_{t\ (Net.1)}^+$: the relative value of total extravasation across the vasculature, $Q_t^-/Q_{t\ (Net.1)}^-$: the relative value of total intravasation across the vasculature, $P_{i(center)}/P_{i(center,Net.1)}$: the relative value of interstitial pressure in the tumor center, $Q_i/Q_{i(Net.1)}$: the relative value of total interstitial flowrate at the tumor margin. 'Net. 2(R),3(R),4(R)' are for 'disrupting randomly' approach, 'Net. 2(S), 3(S), 4(S)' for 'disrupting according to network structure' approach, 'Net. 2(M), 3(M), 4(M)' for 'disrupting according to vessel maturity' approach, 'Net. 2(F), 3(F), 4(F)' for 'disrupting according to blood flowrate' approach. These results show that tumor blood perfusion after vascular-disrupting treatments are mostly declining, except the case of 'Net 2(F)'. Some experimental researches also indicated that vascular-disrupting therapies could either cut down or increase blood perfusion inside of tumors, which depends on the strategy and extent of treatments. E.g. the animal experiments predicted that tumor blood perfusion was obviously declined after the vascular-disrupting treatment using the agent CA-4 [18]. The clinical research also predicted that the local blood flow inside of the breast tumor was rising after vascular-disrupting by anti-VEGF TKRi, see Fig. 10 (provided by Dr A.R. Padhani of Paul Strickland Scanner Centre, UK).

Due to the different disrupting approaches, the vascular densities between the 4 groups are not same. Since some flow variables (e.g. Q_V, Q_t^+, Q_t^-) are directly related to the vascular density, we do not compare the corresponding values between the groups quantitatively, but adopt the qualitative comparison within the same group. We take the curve of $Q_V/Q_{V(Net.1)}$ as the base line, a good perfusion condition can be the combination of : $Q_t^+/Q_{t\ (Net.1)}^+ > Q_V/Q_{V(Net.1)}$; $Q_t^-/Q_{t\ (Net.1)}^- < Q_V/Q_{V(Net.1)}$; and $P_{i(Center)}/P_{i(Center,Net.1)} < Q_V/Q_{V(Net.1)}$. Fig. 11 shows the qualitative comparison of the flows. According to the above criterion, the flow condition of "vascular-disrupting according to flowrate" group is the best (Fig. 11d), especially for the case of 'Network 2(F)' not only Q_t^+ has a rising, Q_t^- reduces to zero, and Q_V increases as well, these changes are helpful to drug delivery inside of tumor.

Table 1: Comparisons of flows on four disrupting vasculatures

	Net. 2(R), 3(R), 4(R)	Net. 2(S), 3(S), 4(S)	Net. 2(M), 3(M),4(M)	Net. 2(F), 3(F),4(F)
$Q_V/Q_{V(Net.1)}$	0.82, 0.52, 0.26	0.90, 0.51, 0.45	0.93, 0.77, 0.57	1.06, 0.65, 0.55
$Q_t^+/Q_{t\ (Net.1)}^+$	0.66, 0.62, 0.25	1.17, 0.80, 0.56	0.95, 0.85, 0.69	1.22, 0.70, 0.56
$Q_t^-/Q_{t\ (Net.1)}^-$	0.46, 0.28, 0.02	0.68, 0.21, 0.07	0.72, 0.34, 0.03	0.007, 0.0, 0.0
$P_{i(center)}/P_{i(center,Net.1)}$	0.75,0.68, 0.42	0.86, 0.71, 0.50	0.93, 0.83, 0.65	0.85, 0.64, 0.45
$Q_i/Q_{i(Net.1)}$	0.72, 0.67, 0.31	0.85, 0.72, 0.44	0.94, 0.83, 0.68	0.82, 0.60, 0.38

$Q_V/Q_{V(Net.1)}$: the relative value of total blood perfusion through the vasculature,
$Q_t^+/Q_{t\ (Net.1)}^+$: the relative value of total extravasation across the vasculature,
$Q_t^-/Q_{t\ (Net.1)}^-$: the relative value of total intravasation across the vasculature,
$P_{i(center)}/P_{i(center,Net.1)}$: the relative value of interstitial pressure in the tumor center,
$Q_i/Q_{i(Net.1)}$: the relative value of total interstitial flowrate at the tumor margin.
'Net. 2(R),3(R),4(R)': for 'disrupting randomly' approach,
'Net. 2(S), 3(S), 4(S)': for 'disrupting according to network structure' approach,
'Net. 2(M), 3(M), 4(M)': for 'disrupting according to vessel maturity' approach,
'Net. 2(F), 3(F), 4(F)': for 'disrupting according to blood flowrate' approach.

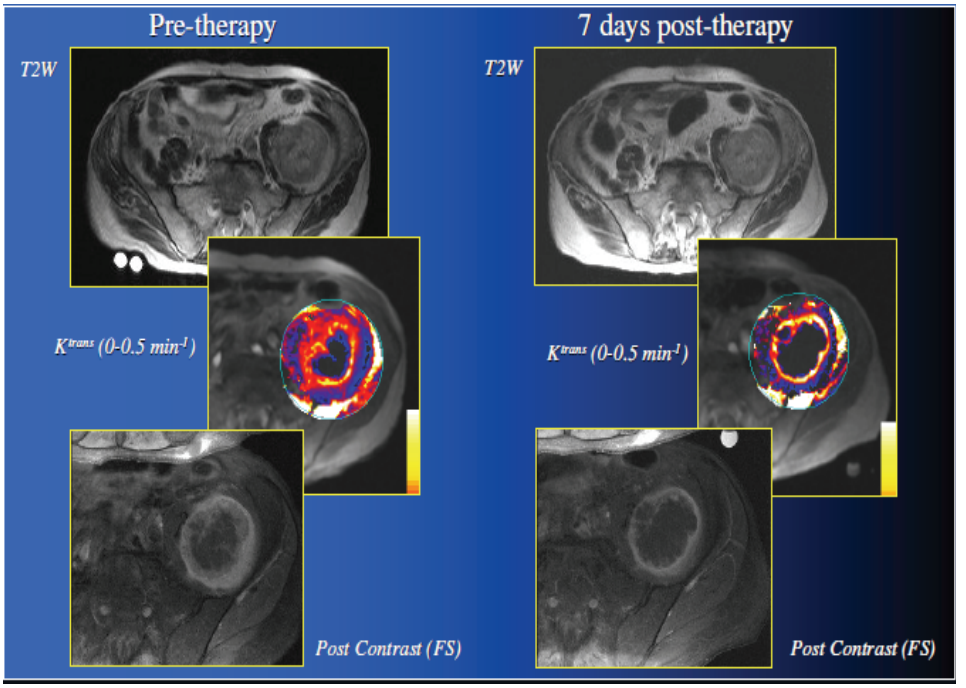

Figure 10: The tumor blood perfusion change before and after the vascular-disrupting treatment (provided by Dr A.R. Padhani of Paul Strickland Scanner Centre, UK).

Additionally, Q_t^+ value in Fig. 11c is generally high, which suggest that disrupting vessels of lower maturity could enhance drug delivery across vasculature. Among the four groups, the effect of "disrupting randomly" group on the flow improvement is relatively poor (Fig. 11a). The above analysis tell us that disrupting some specific vessels may result in better effects on normalization of tumor microenvironment.

4 Discussion

4.1 Model validation: comparisons with the clinical MRI results

There is no technique available on measuring blood flow in such a complex system to provide direct validation of the simulation result. Dynamic Contrast Enhanced MRI (DCE-MRI), however, is able to provide contrast agent perfusion variation with time in *in vivo* tumor microvasculature. In similar manor, a low molecular tracer can be injected into the simulation network and the tracer perfusion curve can be calculated in the simulation. The comparison between the two perfusion

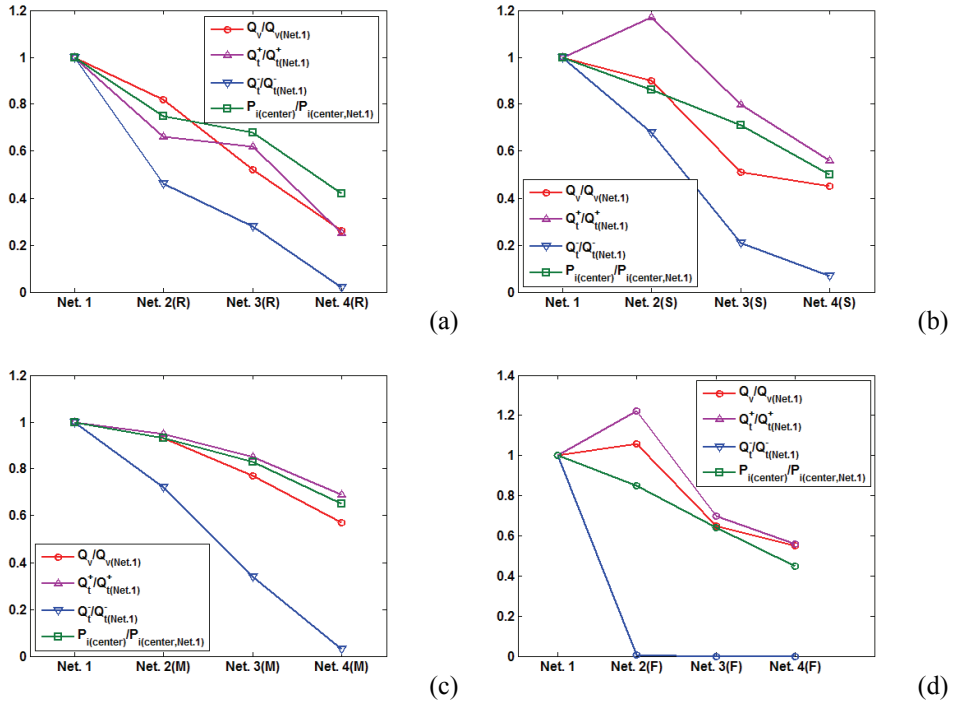

Figure 11: The relative change of the flow variables—the total blood perfusion through the vasculature ($Q_V/Q_{V(Net.1)}$), the total extravasation across the vasculature ($Q_t^+/Q_{t\ (Net.1)}^+$), the total intravasation across the vasculature ($Q_t^-/Q_{t\ (Net.1)}^-$), the interstitial pressure in the tumor center ($P_{i(center)}/P_{i(center,Net.1)}$) , between the same disrupting group, relatively. (a) group of disrupting randomly; (b) group of disrupting according to network structure; (c) group of disrupting according to vessel maturity; (d) group of disrupting according to blood flowrate.

curves will provide validation information qualitatively.

In doing so, a chemotherapy drug is used as an injected tracer in the systems and the concentration profiles of the drug is traced in the network. The transport of the drug through the vascular network and tumor interstitial space are governed by the convection and convective-diffusion equations respectively as follows. Perfect mixing is assumed and no reaction kinetics are considered,

$$\frac{\partial C_p}{\partial t} + \nabla \cdot [R_f U_V C_p] = -K_e \cdot C_p - \phi_s \tag{1}$$

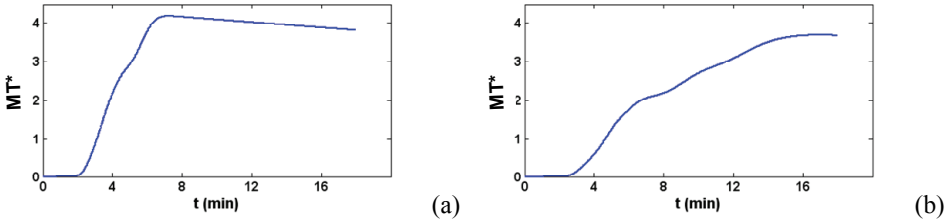

Figure 12: Simulation results of the time-drug mass curve of MT*. (a) before treatment (on Network 1); (b) after treatment (on Network 2(R)).

$$\frac{\partial C_i}{\partial t} + \nabla \cdot [R_f U_i C_i] = \nabla \cdot (D_C \nabla C_i) + \phi_s \tag{2}$$

where C_p and C_i are the solute concentration in plasma and in interstitial fluid respectively. U_V and U_i are the fluid velocity in vessels and in interstitial space respectively. R_f is the retardation factor (the ratio of the solute velocity to the fluid velocity). A correlation from Swabb et al. (1974)[19] yields a value of R_f that is essentially equal to 1.0 for tumor tissue, therefore R_f is assumed to be equal to unity in this analysis. K_e is the drug elimination rate in plasma. D_C is the diffusion coefficient, which is assumed as constant here. ϕ_s is the solute source term, obtained using the equation for transcapillary exchange by Kedem & Katchalsky (1958)[20],

$$\phi_s(x,y,t) = \gamma_s P_{eff} \frac{S}{V} [C_p(x,y,t) - C_i(x,y,t)] \cdot A(x,y) \tag{3}$$

where P_{eff} is the effective vascular permeability coefficient and γ_s is the ratio coefficient. The other terms are the same as in the flow model.

We choose 'Network 1' and 'Network 2(R)' as the vasculatures before and after the vascular-disrupting treatment, respectively. The chemotherapy drug at concentration C_{max} is injected into the arteriole parental vessel, delivered at t =0 and lasting for 120 seconds. Data are collected corresponding to the total dimensionless mass taken up by the tumor tissue (MT*= total drug mass in the tumor / drug mass injected into the parent vessel in one second).

Fig. 12a is the time-drug mass curve of MT* before treatment (on 'Network 1'). It shows a rapid enhancement in the beginning and gradual washout over a 16-min period. Fig. 12b is the corresponding result after treatment (on 'Network 2(R)'). It shows a much slower accumulation of drug within the tumor and minimal washout over a 16-min period. One of the MRI results is shown in Fig. 13, which is the time-contrast agent perfusion curve of MRI on breast cancer before and after treatment[6]. It presents a similar changing trend as the above simulation result. Due

to the differences in tumor size and capillary network structures, the time and solute concentration of the two curves (Fig. 12 and Fig. 13) are accordingly different, the similarity is striking.

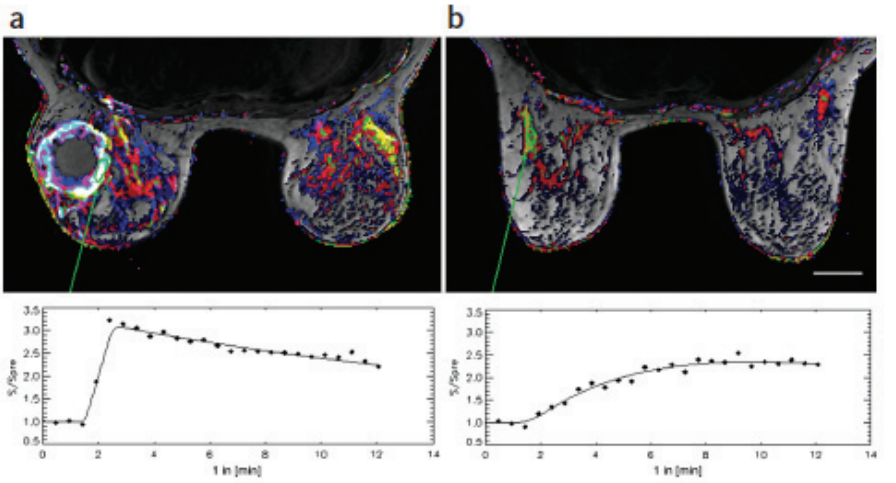

Figure 13: MRI results of the time-contrast agent perfusion curve on breast cancer [6]. (a) before treatment, (b) after treatment.

4.2 Flow states in respond to changes of transport properties of tumor vessels and tissue

Preclinical and clinical evidence shows that some vascular-targeted agents can change tumor vessel permeability, vascular density or some other transport properties of tumor vasculature and interstitium in a process of "normalization" of tumor microenvironment. The elevated interstitial fluid pressure (IFP) is a reflection of the global pathophysiology of solid tumors [2]. In order to investigate how tumor microenvironment are affected by changes in these properties, the sensitivity analysis of the flows are studied in this part, as shown in Fig. 14. The parameters tested are: (a) hydraulic permeability of tumor vessel wall $L_{pV,T}$; (b) hydraulic conductivity of tumor interstitium K_T; (c) absorption capacity of lymphatic system, $L_{pL}S_L/V$. In these figures, superscript '*' denotes the computational results with all baseline parameter values, which is listed in Appendix B.

Fig. 14a shows the change of the flow terms with $L_{pV,T}$ ranging from $10^{-3}L_{pV,T}$* to $10^{3}L_{pV,T}$*. According to the figure, decreasing $L_{pV,T}$ can effectively flatten the plateau of P_i inside of tumor, and also decrease the transvascular leakiness Q_t.

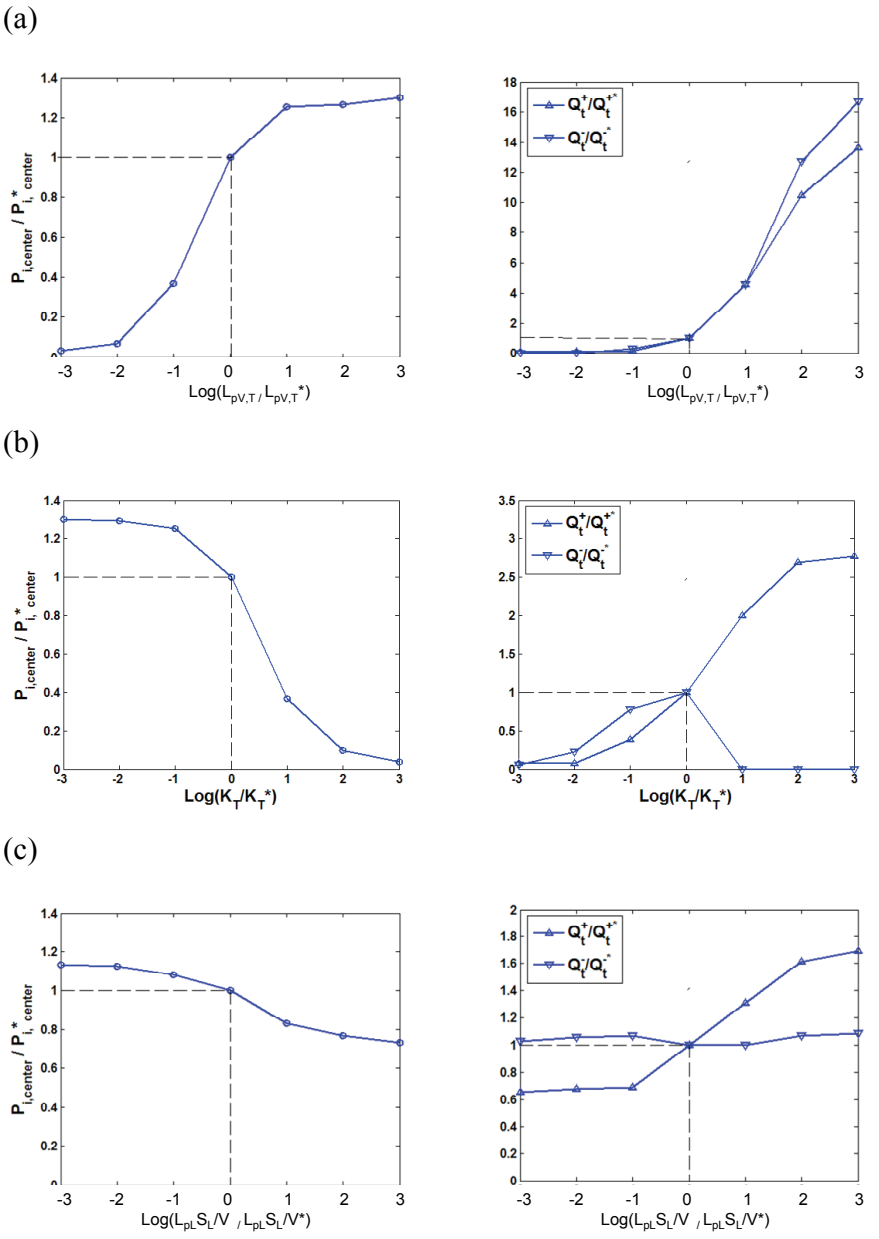

Figure 14: Change of the interstitial pressure P_i in the tumor center ($P_{i,center}/P_{i,center}^*$) and the totaltransvascular flux Q_t through the vasculature (Q_t^+/Q_t^{+*},Q_t^-/Q_t^{-*}), with (a) hydraulic permeability of tumor blood vessel wall $L_{PV,T}$; (b) hydraulic conductivity of tumor interstitium K_T; (c)lymphatic absorption capacity $L_{PL}S_L/V$.

These results indicate that decreasing $L_{pV,T}$ is helpful to relieving the plateau of tumor IFP, reducing the interstitial fluid leakiness into the peri-tumor tissue, as well as preventing the tumor cell metastasis through the intravasation inside the tumor. According to Fig. 14b, the elevated interstitial pressure P_i will be relieved with increasingK_T; Q_t^+ is enhanced with the increasing K_T, while nearly no intravasation occurs once K_T is larger than $10K_T$*. According to Fig.14c, the flows in the normal tissue are more sensitive to the change of $L_{PL}S_L/V$ rather than those inside of the tumor. In the tumor tissue, the high IFP can be lowered but not be flattened totally no matter how large value $L_{pL}S_L/V$ is increased, also, Q_t are not affected greatly with the changes of $L_{pL}S_L/V$. So, there is not remarkable effects on normalizing the tumor microenvironment by the changes in $L_{pL}S_L/V$, compared with those by changing $L_{pV,T}$ and $K_{T.}$

4.3 Limitations

Vessel collapse and regression are commonly observed in solid tumors, which is one of the abnormal characteristics of tumor vessels [2]. Researches showed that the factors leading to vessel collapse in tumors are mechanical stresses generated by the growing tumor itself (pressure) [21] and reduced perfusion of certain vessels (lower wall shear stress) [22]. In the modeling study, Bartha & Rieger (2006) [23] used wall shear stress (WSS) as a criteria of vessel collapse, based on the experimental evidences showing that the long term reduction of vascular shear stress promotes vessel collapse and regression [24]. However, further studies about the mechanism and quantitative researches of the influence of WSS on the angiogenesis are required in the future. In the present work, we have not included the WSS induced vessel collapse mechanism in angiogenesis. However, vessel compliance was simulated by using a typical constitutive mechanical relation for tumor vessels of Netti et al. (1996) [16]. Because lack of feedback mechanism for vessel regression (or collapse), predefined vessel branching probabilities, which is controlled by the tumor location and local chemical-mechanical environment, were used in order to produce a realistic network. When the vessel sprouts grow into the tumor, the migration will be adjusted by the functions. Also, the distribution of TAFs initial concentration was given accordingly. However, these factors are set to be constant during the angiogenesis process, rather than a more realistic dynamic situation. The current model is being improved according to the limitation.

Recently, some works considering the dynamic feedback of tumor growth to the angiogenesis have been published. Lowengrub and co-workers described an avascular tumor growth model in the papers [25–27]. The growth model incorporated the effects of the interaction between the genetic characteristics of the tumor and its microenvironment on the resulting tumor progression and morphology. Rieger

et al. made the simulation of transformation of regular normal vasculature into a highly inhomogeneous tumor capillary network by the model they developed, which combined a dynamically evolving network in the presence of a dynamically changing tumor [23,28]. In our latest development of the tumor growth during vascular-targeted therapies, vessel regression and blood perfusion are all included in a coupled model. Some of the results will be published soon.

5 Conclusion

In this study, we generated tumor "normalized" microvasculature by "vascular-disrupting" treatments, and made the flow simulations on these networks to investigate the effects of vascular-disrupting therapies on tumor microenvironmental flow. Four disrupting approaches were designed according to the abnormal characteristics of tumor microvaculature compared with the normal one. In regard to the flow analysis, since the vascular density of networks between the different disrupting groups are not same, we did not compare the corresponding flow values between the four groups quantitatively, but adopt the qualitative comparison within the same group. The results predict that the vascular-targeted therapies could improve tumor microenvironment, eliminate drug barrier and inhibit metastasis of tumor cells to some extent. Disrupting certain types of vessels may get better effects. In this study, the flow condition on the networks with "vascular-disrupting according to flowrate" is the best comparing with the other three groups, and disrupting vessels of lower maturity could effectively enhance fluid transport across vasculature into interstitial space.

Acknowledgement: This research is supported by the National Natural Science Foundation of China (No.11102113), Postdoctoral Foundation of China (20100470702). State Key Laboratory of Ocean Engineering of independent research project (GP010820).

References

1. Jain, R. K., Tong, R.T., & Munn, L.L. (2007) Effect of vascular normalization by antiangiogenic therapy on interstitial hypertension, peritumor edema, and lymphatic metastasis: Insights from a mathematical model. Cancer Res. 67(6), 2729-2735.

2. Fukumura, D., Jain, R. K. (2007) Tumor microvasculature and microenvironment: targets for anti-angiogenesis and normalization. Microvas. Res. 74, 72–84.

3. Wu, J., Xu, S. X., Long, Q., Padhani, A. R., & Jiang, Y. P. (2008) Simulation of 3D solid tumor angiogenesis including arteriole, capillary and venule. MCB. 5(4), 127-227.

4. Wu, J., Long, Q., Xu, S. X., & Padhani, A. R. (2009) Study of tumor blood perfusion and its variation due to vascular normalization by anti-angiogenic therapy based on 3D angiogenic microvasculature. J. Biomech. 42, 712–721.

5. Chang, Y. S., di Tomaso, E., McDonald, D. M., Jones, R., Jain, R. K., & Munn, L. L. (2000) Mosaic blood vessels in tumors: frequency of cancer cells in contact with flowing blood. Proc. Natl. Acad. Sci. USA. 97, 14608–14613.

6. McDonald, D. M., Choyke, P. L. (2003) Imaging of angiogenesis: from microscope to clinic. Nat. Med. 9, 713–725.

7. di Tomaso, E., Capen,D., Haskell, A., Hart, J., Logie, J. J., Jain, R. K., McDonald, D. M., Jones, R., & Munn, L. L. (2005) Mosaic tumor vessels: cellular basis and ultrastructure of focal regions lacking endothelial cell markers. Cancer Res. 65, 5740–5749.

8. Jain, R. K. (1988) Determinants of tumor blood flow: a review. Cancer Res. 48, 2461-2658.

9. Jain, R. K. (2003) Molecular regulation of vessel maturation. Nat. Med. 9, 685-693.

10. Liu, Z. F., Sun, Y. Y., Kong, Y. W. (2003) The microvessel density and expressions of α2smooth muscle actin in ovarian cancers and their clinical significance. Prog. Obstet. Gynecol. 12(5), 373-375. (in Chinese)

11. Benjamin, L. E., Golijanin, D., Itin, A., Pode, G., & Keshet, E. (1999) Selective ablation of immature blood vessels in established human tumors follows vascular endothelial growth factor with drawal. J. Clin. Invest. 103(2), 159-165.

12. Darland, D. C., D'Amore, P. (1999) Blood vessel maturation: Vascular development comes of age. J. Clin. Invest. 103(2), 157-158.

13. Ste'phanou, A., McDougall, S. R., Anderson, A. R. A., & Chaplain, M. A. J. (2005) Mathematical modelling of flow in 2D and 3D vascular networks: applications to anti-angiogenic and chemotherapeutic drug strategies. Math. Comput. Model. 41, 1137-1156.

14. Wu, J., Xu, S. X., Long, Q., Collins, M. W., König, C. S., Zhao, G. P., Jiang, Y.P., & Padhani, A. R. (2008) Coupled modeling of blood perfusion in intravascular, interstitial spaces in tumor microvasculature. J. Biomech. 41, 996-1004.

15. Pries, A. R., Secomb, T. W., Gessner, T., Sperandio, M. B., Gross, J. F., & Gaehtgens, P. (1994) Resistance to blood flow in microvessels in vivo. Circulation Res. 75, 904–915.

16. Netti, P. A., Roberge, S., Boucher, Y., Baxter, L. T., & Jain, R. K. (1996) Effect of transvascular fluid exchange on pressure–flow relationship in tumors: a proposed mechanism for tumor blood flow heterogeneity. Microvas. Res. 52, 27–46.

17. Pries, A. R., Secomb, T. W. (2005) Microvascular blood viscosity in vivo and the endothelial surface layer. Am. J. Physiol. Heart Circ. Physiol. 289, 2657–2664.

18. Tozer, G. M., Prise, V. E., Wilson, J., Locke, R. J., Vojnovic, B., Stratford, M. R. L., Dennis, M. F., & Chaplin, D. J. (1999) Combretastatin A-4 Phosphate as a tumor vascular- targeting agent: early effects in tumors and normal tissues. Cancer Res. 59, 1626-1634.

19. Swabb, E. A., Wei, J., Gullino, P. M. (1974) Fluid and protein fluxes across small and large pores in the microvasculature. Application of two-pore equations. Acta. Physiol. Scand. 131, 441-428.

20. Kedem, O., Katchalsky, A. (1958) Thermodynamic analysis of permeability of biological membranes to non-electrolytes. Biochim. Biophs. Acta. 27, 229-246.

21. Griffon-Etienne, G., Boucher, Y., Brekken, C., Suit, H. D., & Jain, R. K. (1999) Taxane-induced apoptosis decompresses blood vessels and lowers interstitial fluid pressure in solid tumors: clinical implications. Cancer Res. 59, 3776-3782.

22. Milkiewicz, M., Brown, M. D., Egginton, S., & Hudlicka, Q. (2001) Association between shear stress, angiogenesis, and VEGF in skeletal muscles in vivo. Microcirculation 8, 229–241.

23. Bartha, K., Rieger, H. (2006) Vascular network remodeling via vessel cooption, regression and growth in tumors. J. Theor. Biol. 241, 903-918.

24. Duval, H., Harris, M., Li, J., Johnson, N., & Print, C. (2003) New insights into the function and regulation of endothelial cell apoptosis. Angiogenesis 6, 171-183.

25. Macklin, P., Lowengrub, J. (2007) Nonlinear simulation of the effect of the microenvironment on tumor growth. J. Theor. Biol. 245, 677-704.

26. Macklin, P., McDougall, S., Anderson, A. R. A., Chaplain, M. A. J., Cristini, V., & Lowengrub, J. (2009) Multiscale modelling and nonlinear simulation of vascular tumour growth. J. Math. Biol. 58, 765-798.

27. Wise, S. M., Lowengrub, J. S., Frieboes, H. B., & Cristini, V. (2008) Three-dimensional multispecies nonlinear tumor growth-I. Model and numerical method. J. Theor. Biol., 253, 524-543.

28. Welter, M., Bartha, K., Rieger, H. (2008) Emergent vascular network inhomogeneities and resulting blood flow patterns in a growing tumor. J. Theor. Biol. 250, 257.

Appendix

Appendix A 3D Model of Tumor Angiogenesis

The model was initially proposed by Anderson & Chaplain (1998) [1*]. It assumed that endothelial cells (ECs) migrate through random motility, chemotaxis in response to tumor angiogenesis factors (TAFs) released by the tumor, and haptotaxis in response to fibronectin (FN) gradients in the excellular matrix. We denote the EC density per unit area e, the TAF concentration c and the FN concentration f. The non-dimensional equations describing the vascular growth process is thus given by,

$$\begin{aligned}
\frac{\partial e}{\partial t} &= \overbrace{D\nabla^2 e}^{random\ motility} - \overbrace{\nabla\cdot(\frac{\chi}{1+\alpha c}e\nabla c)}^{chemotaxis} - \overbrace{\nabla\cdot(\rho e\nabla f)}^{haptotaxis} \\
\frac{\partial f}{\partial t} &= \overbrace{\beta e}^{production} - \overbrace{\gamma e f}^{uptake} \\
\frac{\partial c}{\partial t} &= -\overbrace{\eta e c}^{uptake}
\end{aligned} \tag{A1}$$

The coefficients D, χ and ρ characterize the random, chemotactic and haptotactic cell migration, respectively. β, γ and η are coefficients describing the rates of FN production, FN degradation and TAF uptake by ECs, respectively.

In order to track the motion of individual endothelial cells located at the sprout tips and the subsequent formation of vessels, the 3D discretized form of the system of partial differential equations is used, obtained by the standard Euler finite difference approximation,

$$\begin{aligned} e_{l,m,n}^{q+1} =& e_{l,m,n}^{q} P_0 + e_{l+1,m,n}^{q} P_1 + e_{l-1,m,n}^{q} P_2 + e_{l,m+1,n}^{q} P_3 \\ &+ e_{l,m-1,n}^{q} P_4 + e_{l,m,n+1}^{q} P_5 + e_{l,m,n-1}^{q} P_6 \\ f_{l,m,n}^{q+1} =& f_{l,m,n}^{q}(1-\Delta t\gamma e_{l,m,n}^{q}) + \Delta t\beta e_{l,m,n}^{q} \\ c_{l,m,n}^{q+1} =& c_{l,m,n}^{q}(1-\Delta t\eta e_{l,m,n}^{q}) \end{aligned} \tag{A2}$$

where l, m, n specify the location on the grid and q is for the time step, i.e. $x = l\Delta x$, $y = m\Delta y$, $z = n\Delta z$ and $t = q\Delta t$. The coefficients $P_0 \sim P_6$ incorporate the effects of random, chemotactic and haptotactic movement and depend upon the local chemical environment (FN and TAF concentrations). They relate to the likelihood of the EC remaining stationary (P_0), or moving along the x(P_1), -x (P_2), y (P_3), -y (P_4), z (P_5), or -z (P_6) axis direction. The full expressions of P_0–P_6 can be found in Wu et al. (2008)[2*].

The process of branching (formation of new sprouts from existing sprout tips) and anastomosis (formation of loops by fusion of two colliding sprouts) are assumed as follows [1*],

For branching:

(1) the likelihood of an existing sprout increases with the local TAF concentration,

(2) a sprout vessel must reach a certain level of maturation before it is able to branch.

For anastomosis:

(1) if two sprouts collide as they grow, only one of them is allowed to keep growing (the choice of which is random),

(2) if a sprout tip meets another sprout, they fuse to form a loop.

The process of splitting large "mother" blood vessels into smaller "daughter" vessels is considered in the present model. The vessel diameter is prescribed by,

$$d_n = g_n d_0 \quad (n = 1, 2, 3 \ldots) \tag{A3}$$

where n is the value of branching generation, d_0 is the diameter of the parent vessels ($d_{0,A}$ for the parental arteriole, $d_{0,V}$ for the parental venule), d_n is the diameter of the n^{th} generation vessels, g_n is the ratio coefficient smaller than 1. We assume that, with continuously branching, the difference of the diameters between

the "mother" vessels (generation n) and their "daughters" (generation $n+1$) decreases monotonously with n, accordingly $g_n$in the above equation is given by,

$$g_{n+1} = \lambda^{\frac{1}{n+1}} g_n \tag{A4}$$

in which λ is a coefficient below 1. Eqs.(A3)$\sim$(A4) is just one reasonable form of controlling vessel diameter, other forms could also be adopted.

In order to analyze the haemodynamics data from the flow simulations, one critical generation n_c is defined to classify the vessels artificially. It is assumed that if the branching generation is beyond n_c, the vessels are viewed as capillaries, otherwise are classified as small arterioles or venules (according to their original parent vessels).

The simulation is carried out on a 3D domain of $2mm \times 2mm \times 2mm$, divided into $100 \times 100 \times 100$ grids. A half tumor with a diameter of $2mm$ is on the left boundary and surrounded by normal tissue of the host, the parental arteriole and venule is located on the right top and right bottom, with diameters of $24\mu m$ and $32\mu m$ respectively, see Fig. 2 in the text.

The initial distribution of FN and TAF concentrations are described by,

$$c(r,0) = \begin{cases} 1 & 0 \le r \le 0.3 \\ \frac{(v-r)^2}{v-0.4771} & 0.3 \le r \end{cases} \tag{A5}$$

$$f(r,0) = \zeta(\exp^{-\frac{(x-1)^2+(z-1)^2}{\varepsilon}} + \exp^{-\frac{(x-1)^2+z^2}{\varepsilon}}) \tag{A6}$$

where r is the dimensionless distance from the tumor center and v =1.07, assuming the tumor has a necrotic region with the radius of $0.6R_T$(corresponding to $r \le 0.3$, R_T is the tumor radius). Zero flux conditions are imposed on the boundaries.

The dimensionless parameter values used for the simulations are [1*,3*,4*]: D=0.00035,α=0.6, χ=0.38, ρ=0.22, β=0.05, γ=0.1, η=0.1,ζ=0.45, ε=0.75, time is scaled as $\tilde{t} = t/\tau$ with $\tau = L/D_c$, where L = $2mm$ is the length of the domain and $D_c = 2.9 \times 10^{-7} cm^2/s$ is taken as the diffusion coefficient for TAF. The detailed description of the model, along with the connectivity examination of the vasculature, the sensitivity analysis of the network architecture to the parameters, and the discussion about the model assumptions, can be found in Wu et al. (2008)[2*].

Appendix B Model of tumor haemodynamics

1. Intravascular blood flow

Assuming flux conservation and incompressible flow at each node$c$,

$$\sum_{k=1}^{6} Q_{(c)}^{k} B_{(c)}^{k} = 0 \tag{B1}$$

$$Q_{(c)}^{k} = Q_{V,(c)}^{k} - Q_{t,(c)}^{k} \tag{B2}$$

where $B_{(c)}^{k}$ is a positive integer, representing the connectivity between node c and its adjacent node k. $B_{(c)}^{k}$=1 or ($B_{(c)}^{k}$=0) means node c and k are connected (or not connected) to form vascular element k. $Q_{(c)}^{k}$ is the flowrate from node k to node c. $Q_{V,(c)}^{k}$ is the intravascular flowrate without fluid leakage, described by local Poiseuille's law,

$$Q_{V,(c)}^{k} = \frac{\pi R_k^4}{8\mu_k} \frac{(P_{V,(k)} - P_{V,(c)})}{\Delta l_k} \tag{B3}$$

$Q_{t,(c)}^{k}$ is the transvascular flowrate, following Starling's law,

$$Q_{t,(c)}^{k} = 2\pi R_k \Delta l_k \cdot L_{pV}(\bar{P}_{V,(c)}^{k} - \bar{P}_{i,(c)}^{k} - \sigma_T(\pi_V - \pi_i)) \tag{B4}$$

where $P_{V,(c)}$, $P_{V,(k)}$ are the intravascular pressure of node c and k, $\bar{P}_{V,(c)}^{k}$ is the mean intravascular pressure in vascular element k, $\bar{P}_{i,(c)}^{k}$ is the mean interstitial pressure outside vascular element k, μ_k is the blood viscosity in vascular element k, Δl_k and R_k are the length and radius of vascular element k (all Δl_k equal to Δl in this paper), L_{pV} is the hydraulic permeability of blood vessel wall, σ_T is the average osmotic reflection coefficient for plasma proteins, π_V and π_i are the colloid osmotic pressure of plasma and interstitial fluid.

2. Interstitial fluid flow

The interstitial fluid flow is modeled by Darcy's law [5*],

$$\vec{U}_i = -K\nabla P_i \tag{B5}$$

$\vec{U}_i$ is the interstitial fluid velocity, K is the hydraulic conductivity coefficient of the interstitium.

The continuity equation is given by,

$$\nabla \cdot \vec{U}_i = \phi_V - \phi_L \tag{B6}$$

ϕ_V is the fluid source term leaking from blood vessels, which is heterogeneously distributed in the interstitial space and described by Starling's law,

$$\phi_V = \frac{L_{pV} S_V}{V}(P_{eV} - P_i) \tag{B7}$$

P_{eV} $(= P_V - \sigma_T(\pi_V - \pi_i))$ is the effective pressure inside blood vessels. s_V/V is the surface area of blood vessel wall per unit volume of tissue. In the present model, s_V/V is considered as a spatial variable as follows,

$$S_V/V = \sum_k 2\pi R_k \cdot \frac{1}{2}\Delta l/\Delta l^3 = \sum_k \pi R_k/\Delta l^2 \tag{B8}$$

ϕ_L is the lymphatic absorption term, prescribed by,

$$\phi_L = \frac{L_{pL}S_L}{V}(P_i - P_{eL}) \cdot F(P_i) \tag{B9}$$

$$F(P_i) = \begin{cases} 1 & P_i \geq P_{eL} \\ 0 & P_i < P_{eL} \end{cases} \tag{B10}$$

P_{eL} is the effective pressure inside lymphatic vessels, L_{pL} is the hydraulic permeability of lymphatic vessel wall, s_L/V is the surface area of lymphatic vessel wall per unit volume of tissue. In the model, $L_{PL}S_L/V$ is assumed zero for tumor tissue, and given a uniform value for normal tissue referring to Baxter & Jain (1990)[6*]. Eq.(B10) represents that no fluid in the lymphatic vessels would filtrate into the interstitium, even if the interstitial pressure is below the lymphatic pressure.

Combing Eqs. (B5)∼(B10),

$$\nabla^2 P_i = \alpha_V^2(P_i - P_{eV}) + \alpha_L^2(P_i - P_{eL}) \cdot F(P_i) \tag{B11}$$

where $\alpha_V = \sqrt{\frac{L_{pV}S_V}{KV}}$,$\alpha_L = \sqrt{\frac{L_{pL}S_L}{KV}}$. The continuity of pressure and flux on the interconnected boundary between the tumor and normal tissue Γ are as follows,

$$P_i|_{\Gamma^-} = P_i|_{\Gamma^+}, \quad -K_T \nabla P_i|_{\Gamma^-} = -K_N \nabla P_i|_{\Gamma^+} \tag{B12}$$

K_N, K_T are the hydraulic conductivity coefficients of normal tissue and tumor tissue, respectively.

3. Vessel Compliance

It is assumed the blood vessels outside tumor are rigid, while the intra-tumoral ones are compliant specified by the equation of Netti et al. (1996) [7*],

$$R = R_{init}(\frac{P_V - P_i + P_c}{E})^b \tag{B13}$$

R is the vessel radius,R_{init} is the initial radius obtained from the angiogenesis simulation, b is the compliance exponent, E is the compliance coefficient, P_c is the collapse pressure.

4. Blood rheology

The formula developed by Pries et al. (1994)[8*] is adapted to describe viscosity changes,

$$\begin{aligned}
\mu &= \mu_{plasma}\left[1+(\mu_{0.45}-1)\frac{(1-H)^c-1}{(1-0.45)^c-1}\left(\frac{2R}{2R-1.1}\right)^2\right]\left(\frac{2R}{2R-1.1}\right)^2 \\
\mu_{0.45} &= 6e^{-0.17R}+3.2-2.44e^{-0.06(2R)^{0.645}} \\
c &= (0.8+e^{-0.15R})\left(-1+\frac{1}{1+10^{-11}(2R)^{12}}\right)+\frac{1}{1+10^{-11}(2R)^{12}}
\end{aligned} \tag{B14}$$

μ_{plasma} is the viscosity of plasma, H is the blood hematocrit.

The distribution of red blood cells (RBCs) at microvascular bifurcations is represented according to the approach proposed by Pries & Secomb (2005)[9*]. The fractional flow of erythrocytes into one daughter branch (FQ_E) is calculated from the respective fractional blood flow (FQ_B) as follows,

$$\begin{aligned}
\mathrm{logit}(FQ_E) &= \Phi_1+\Phi_2\log it\left(\frac{FQ_B-\Phi_3}{1-2\Phi_3}\right) \\
\Phi_1 &= -13.29[(d_\alpha^2/d_\beta^2-1)/(d_\alpha^2/d_\beta^2+1)](1-H_m)/d_m \\
\Phi_2 &= 1+6.98(1-H_m)/d_m \\
\Phi_3 &= 0.964(1-H_m)/d_m
\end{aligned} \tag{B15}$$

where logit x= ln[x/(1- x)]. Parameter$\Phi_1$describes the difference between the relations derived for the two daughter branches, $\Phi_2$denotes the nonlinearity of the relation between FQ_E and FQ_B, and Φ_3 defines the minimal fractional blood flow required to draw RBCs into the daughter branch, where d_α,d_β and d_m are the diameters of the daughter branches and the mother vessel, H_m is the discharge hematocrit in the mother vessel. In these relations, all diameters are given in micrometers.

The parameter values are listed in Table A. The numerical procedure is given in the following section.

5. Numerical Procedure

5.1 Iterative algorithm for the intravascular pressure

Table Table A: Parameter Values Used In Flow Simulations

Parameter	**Value**	**Parameter**	**Value**
$P_{V,A}(mmHg)^{**}$	25	$P_{V,V}(mmHg)^{**}$	10
$d_{0,A}(\mu m)^{**}$	24	$d_{0,V}(\mu m)^{**}$	32
$L_{PV}(cm/mmHg\text{-}s)^{[11*]}$	Normal: 3.6×10^{-8} Tumor: 1.86×10^{-6}	$L_{PL}S_L/V\ (1/mmHg\text{-}s)^{**}$	Normal: 1.0×10^{-4} Tumor: 0
$K(cm^2/mmHg\text{-}s)^{[11*]}$	Normal: 2.5×10^{-7} Tumor: 2.5×10^{-7}	$\sigma_T^{[11*]}$	Normal: 0.91 Tumor: 8.7×10^{-5}
$\pi_V\ (mmHg)^{[11*]}$	Normal: 20 Tumor: 19.8	$\pi_i\ (mmHg)^{[11*]}$	Normal: 10 Tumor: 17.3
μ_{plasma}(cP)$^{[12*]}$	1.2	$H_D^{[13*]}$	0.45
$P_{eL}(mmHg)^{**}$	Normal: 0.5	$P_c\ (mmHg)^{[7*]}$	3.0
$b^{[7*]}$	0.1	$E\ (mmHg)^{[7*]}$	6.5

**estimated according to the physiological condition at microvascular scale.

Combining Eqs. (B1)∼(B4), the iterative solution for $P_{V,(c)}$ is,

$$P_{V,(c)}^{q+1} = \frac{\left(\begin{array}{l} \sum_{k=1}^{6} \{ (\frac{R_k^4}{8\mu_k \Delta l} - R_k \Delta l \cdot L_{pV}) P_{V,(k)}^q \\ +2R_k \Delta l \cdot L_{pV} [\bar{P}_{i,(c)}^k + \sigma_T(\pi_V - \pi_i)] \} \cdot B_{(c)}^k \end{array} \right)}{\left(\sum_{k=1}^{6} (\frac{R_k^4}{8\mu_k \Delta l} + R_k \Delta l \cdot L_{pV}) \cdot B_{(c)}^k \right)} \tag{B16}$$

where q is the number of iterations. After stability analysis, the iteration satisfies the convergence condition. The iteration continues until the relative error $\sum \left| P_{V,(c)}^{q+1} - P_{V,(c)}^q \right| / \sum \left| P_{V,(c)}^{q+1} \right|$ decreases to $\leq 10^{-6}$, indicating a converged solution is reached.

5.2 Iterative algorithm for the interstitial pressure

Eq.(B11) is discretized by *Forward Temporal and Center Spatial (FTCS)* finite difference scheme and solved by *Successive Over Relaxation (SOR)* iteration method with a space step $\Delta x = \Delta y = \Delta z = \Delta l$,

$$\begin{aligned} P_{i(l,m,n)}^{q+1} &= P_{i(l,m,n)}^q + \frac{\omega}{6 + \Delta l^2 \alpha_{V(l,m,n)}^2 + \Delta l^2 \alpha_L^2 F(P_{i(l,m,n)}^q)} \\ &\cdot [P_{i(l+1,m,n)}^q + P_{i(l-1,m,n)}^q + P_{i,(l,m+1,n)}^q + P_{i,(l,m-1,n)}^q + P_{i,(l,m,n+1)}^q + P_{i,(l,m,n-1)}^q \\ &+ \Delta l^2 \alpha_{V(l,m,n)}^2 P_{eV(l,m,n)} + \Delta l^2 \alpha_L^2 P_{eL} F(P_{i(l,m,n)}^q) \\ &\quad - (6 + \Delta l^2 \alpha_{V(l,m,n)}^2 + \Delta l^2 \alpha_L^2 F(P_{i(l,m,n)}^q)) \cdot P_{i(l,m,n)}^q] \end{aligned} \tag{B17}$$

where l,m,n specify the location on the grid, q is the iteration number, ω is the relaxation factor chosen for the convergence condition. The iteration process continues until the relative error $\sum \left| P_{i,(l,m,n)}^{q+1} - P_{i,(l,m,n)}^q \right| / \sum \left| P_{i,(l,m,n)}^{q+1} \right|$ decreases to $\leq 10^{-6}$, indicating a converged solution is reached.

5.3 Iterative steps for the microcirculation simulation

(1) Give the boundary values $P_{V,A}$, $P_{V,V}$—the intravascular pressure of the parental arteriole and venule, see Fig. 2b in the text. A set of initial solutions P_V^o, P_i^o, R^o, μ^o is also prescribed.

(2) Compute P_V, P_i and their relative errors

$$errP_V = \sum \left| P_V^- P_V^o \right| / \sum P_V, \quad errP_i = \sum |P_i - P_i^o| / \sum P_i$$

by the iteration computations described above, respectively.

(3) Update R and its relative error $errR = \sum |R - R^o| / \sum R$.

(4) Compute H by using Eq. (B15).

(5) Updateμ and its relative error $err\mu = \sum|\mu - \mu^o|/\sum\mu$.

(6) Calculate the maximum error err=max($errP_V$, $errP_i$, $errR$, $err\mu$). The new set of solutions is fed back into step (2) with $P_i \Rightarrow P_V^o$, $P_V \Rightarrow P_i^o$, $R \Rightarrow R^o$, $\mu \Rightarrow \mu^o$ and the corresponding flow pattern computed.

(7) Repeat steps (2)$\sim$(6) until $err \leq 1e^{-6}$, indicating the microcirculation reaches the steady state. This value is chosen empirically to optimize the overall performance of the simulations.

References

1* Anderson, A. R. A., Chaplain, M. A. J. (1998) Continuous and discrete mathematical models of tumor-induced angiogenesis. Bull. Math. Biol. 60, 857–900.

2* Wu, J., Xu, S. X., Long, Q., Padhani, A. R., & Jiang, Y. P. (2008) Simulation of 3D solid tumor angiogenesis including arteriole, capillary and venule. MCB. 5(4), 127-227.

3* Ste'phanou, A., McDougall, S. R., Anderson, A. R. A., & Chaplain, M. A. J. (2005) Mathematical modelling of flow in 2D and 3D vascular networks: applications to anti-angiogenic and chemotherapeutic drug strategies. Math. Comput. Model. 41, 1137-1156.

4* Ste'phanou, A., McDougall, S., Anderson, A. R. A, & Chaplain, M.A.J. (2006) Mathematical modelling of the influence of blood rheological properties upon adaptive tumor-induced angiogenesis. Math. Comput. Model. 44, 96-123.

5* Baxter, L. T., Jain, R. K. (1989) Transport of fluid and macromolecules in tumors. I. Role of interstitial pressure and convection. Microvascular Res. 37, 77–104.

6* Baxter, L. T., Jain, R. K. (1990) Transport of fluid and macromolecules in tumors. II.Role of heterogeneous perfusion and lymphatics. Microvascular Res. 40, 246-263.

7* Netti, P. A., Roberge, S., Boucher, Y., Baxter, L. T., & Jain, R. K. (1996) Effect of transvascular fluid exchange on pressure–flow relationship in tumors: a proposed mechanism for tumor blood flow heterogeneity. Microvas. Res. 52, 27–46.

8* Pries, A. R., Secomb, T. W., Gessner, T., Sperandio, M. B., Gross, J. F., & Gaehtgens, P. (1994) Resistance to blood flow in microvessels in vivo. Circulation Res. 75, 904–915.

9* Pries, A. R., Secomb, T. W. (2005) Microvascular blood viscosity in vivo and the endothelial surface layer. Am. J. Physiol. Heart Circ. Physiol. 289, 2657–2664.

10* Jain, R.K., Tong, R. T., Munn, L.L. (2007) Effect of vascular normalization by antiangiogenic therapy on interstitial hypertension, peritumor edema, and lymphatic metastasis: Insights from a mathematical model. Cancer Research 67: (6), 2729-2735.

11* Fung, Y.C. (1986) Blood rheology in microvessels. In: He, X.X. (Ed.), Biomechanics—Mechanical Properties of Living Tissues. Hunan Science Technique Publisher, China, pp. 157–197.

12* Alarcon, T., Byrneb, H.M., Mainia, P.K. (2003) A cellular automaton model for tumor growth in inhomogeneous environment. Journal of Theoretical Biology, 225, 257–274.